THE JOURNAL OF PHYSICAL CHEMISTRY B

Article

pubs.acs.org/JPCB

Assessing the Performance of MM/PBSA and MM/GBSA Methods. 3. The Impact of Force Fields and Ligand Charge Models

Lei Xu,[†] Huiyong Sun,[‡] Youyong Li,[‡] Junmei Wang,[§] and Tingjun Hou*[,†,‡]

[†]College of Pharmaceutical Sciences, Zhejiang University, Hangzhou, Zhejiang 310058, China

[‡]Institute of Functional Nano & Soft Materials (FUNSOM) and Jiangsu Key Laboratory for Carbon-Based Functional Materials & Devices, Soochow University, Suzhou, Jiangsu 215123, China

[§]Department of Biochemistry, The University of Texas Southwestern Medical Center, 5323 Harry Hines Blvd., Dallas, Texas 75390, United States

Supporting Information

ABSTRACT: Here, we systematically investigated how the force fields and the partial charge models for ligands affect the ranking performance of the binding free energies predicted by the Molecular Mechanics/Poisson−Boltzmann Surface Area (MM/PBSA) and Molecular Mechanics/Generalized Born Surface Area (MM/GBSA) approaches. A total of 46 small molecules targeted to five different protein receptors were employed to test the following issues: (1) the impact of five AMBER force fields (ff99, ff99SB, ff99SB-ILDN, ff03, and ff12SB) on the performance of MM/GBSA, (2) the influence of the time scale of molecular dynamics (MD) simulations on the performance of MM/GBSA with different force fields, (3) the impact of five AMBER force fields on the performance of MM/PBSA, and (4) the impact of four different charge models (RESP, ESP, AM1-BCC, and Gasteiger) for small molecules on the performance of MM/PBSA or MM/GBSA. Based on our simulation results, the following important conclusions can be obtained: (1) for short time-scale MD simulations (1 ns or less), the ff03 force field gives the best predictions by both MM/GBSA and MM/PBSA; (2) for middle time-scale MD simulations (2−4 ns), MM/GBSA based on the ff99 force field yields the best predictions, while MM/PBSA based on the ff99SB force field does the best; however, longer MD simulations, for example, 5 ns or more, may not be quite necessary; (3) for most cases, MM/PBSA with the Tan's parameters shows better ranking capability than MM/GBSA (GB^{OBC1}); (4) the RESP charges show the best performance for both MM/PBSA and MM/GBSA, and the AM1-BCC and ESP charges can also give fairly satisfactory predictions. Our results provide useful guidance for the practical applications of the MM/GBSA and MM/PBSA approaches.

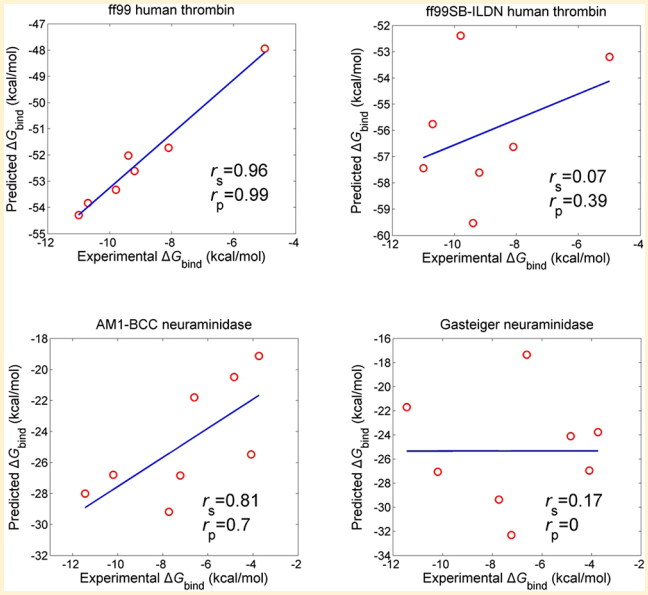

INTRODUCTION

The MM/PBSA and MM/GBSA approaches based on MD simulations have been extensively used in the prediction of binding free energies.[1−22] Both of these two approaches can rigorously decompose the total binding free energy into different interaction terms.[23−25] They are more computationally efficient than the more rigorous methods such as free energy perturbation (FEP) and thermodynamic integration (TI).[3,26,27] The binding free energy for a protein−ligand complex is calculated by MM/PBSA or MM/GBSA using the following equations:

$$\Delta G_{bind} = G_{com} - (G_{rec} + G_{lig}) \quad (1)$$

$$\Delta G_{bind} = \Delta H - T\Delta S \approx \Delta E_{MM} + \Delta G_{sol} - T\Delta S \quad (2)$$

$$\Delta E_{MM} = \Delta E_{internal} + \Delta E_{electrostatic} + \Delta E_{vdw} \quad (3)$$

$$\Delta G_{sol} = \Delta G_{PB/GB} + \Delta G_{SA} \quad (4)$$

where ΔG_{bind} represents the binding free energy of receptor and ligand, and it is the summation of the changes of the gas phase molecular mechanical energy (ΔE_{MM}), the desolvation free energy (ΔG_{sol}), and the conformational entropy ($-T\Delta S$) upon association of ligand. ΔE_{MM} contains the internal energy term ($\Delta E_{internal}$, the summation of bond, angle, and dihedral energies), the electrostatic energy term ($\Delta E_{electrostatic}$), and the van der

Received: April 27, 2013
Revised: June 20, 2013
Published: June 21, 2013

   dx.doi.org/10.1021/jp404160y | J. Phys. Chem. B 2013, 117, 8408−8421

Waals energy term (ΔE_{vdw}). ΔG_{sol} is the sum of the electrostatic ($\Delta G_{PB/GB}$, polar) and nonelectrostatic (ΔG_{SA}, nonpolar) components. The polar contribution of desolvation is computed by implicit solvation models, such as Poisson−Boltzmann (PB) and generalized Born (GB) approaches. PB employs a more rigorous algorithm than GB,[28] but the GB parameters have always been optimized by fitting experimental data.[29−31] Therefore, it is not easy to judge which one is better, because they show conflicting performance for different systems.[23,32,33]

By applying MM/GBSA or MM/PBSA, the energy components are computed from a set of conformational snapshots taken from MD simulations. It is well-known that force field is the cornerstone for MD simulation, and a large number of force fields have been developed by fitting parameters to data from quantum-level calculations and/or experimental data. For instance, the AMBER force fields in the AMBER molecular simulation package have many different versions, such as ff94,[34] ff99,[35] ff99SB,[36] ff99SB-ILDN,[37] ff03,[38] and the latest one, ff12SB.[39] Generally, the newer version of a force field will be more suitable for some specific questions due to the improvement of the corresponding features. For example, with respect to ff94 force field the ff99 force field includes an extra Fourier component to the torsional energy term to achieve a better fitting for conformational energies.[35] In order to overcome the defect of the overstabilization of proteins, the force field parameters for the backbone and side-chain torsion potentials in the ff99SB and ff99SB-ILDN force fields were improved;[36,37] by fitting the data from quantum-level calculations with continuum solvent models. The ff03 force field was designed to give better descriptions for macromolecules in condensed-phase.[38] In order to enhance the prediction accuracy for secondary structure propensities over ff99SB, the protein backbone and side chain dihedral corrections were updated for the ff12SB force field.[39]

It may be considered that the latest force field can give better prediction for binding affinities than the older ones. Unfortunately, as discussed below, the latest force field may not give better performance than the older versions for the binding free energies predicted by MM/PBSA or MM/GBSA, because the fitting for new force field parameters primarily emphasizes the conformations and dynamics of proteins, not the binding free energies.[36,37]

Partial atomic charges also play a very important role in MD simulations. The partial charges for proteins are usually afforded by the employed force field, but there are no widely accepted standards specifying which type of partial charges should be used for arbitrary small molecules. The restrained electrostatic potential (RESP) charges,[40] which are corrected from the electrostatic potential (ESP) charges,[41] have been widely employed in MD simulations based on the AMBER force fields. Another charge model based on semiempirical quantum calculations, named AM1-BCC (AM1 with bond charge corrections) charges,[42] which have been parametrized on small organic molecules to reproduce the RESP charges, have shown promising capability to predict small-molecule hydration free energies[43] and protein−ligand binding affinities.[44] By taking advantage of a set of well prepared parameters based on *ab initio* calculations, deriving the AM1-BCC charges is much more time-saving than deriving the RESP or ESP charges. One charge model that is supported by the antechamber module in the Amber molecular simulation package is the Gasteiger charge,[45] and it has been widely used in virtual screening due to its high computational efficiency. The Gasteiger charges are not derived from electrostatic potentials based on quantum-level calculations, and only depend on the connectivity of the atoms in a molecule.[45]

Various studies have been performed to investigate the influence of different protocols and parameters on the predictions of MM/PBSA and MM/GBSA.[32,46−48] For example, we have systematically investigated the impact of the time scale of MD simulations, the solute dielectric constant, the entropy calculations, and the different PB or GB models for computing electrostatic desolvation on the performances of the MM/PBSA and MM/GBSA approaches.[32] In the following study, we investigated the performance of MM/PBSA and MM/GBSA to identify the correct binding poses and rank the binding free energies for an extensive set of protein−ligand complexes.[46] Recently, Genheden and co-workers evaluated the performance of different protocols by calculating the entropy term with a normal-mode analysis of harmonic frequencies in the MM/GBSA and MM/PBSA approaches.[48] Weis et al. studied how the force fields affect the binding free energies for seven biotin analogues, but they did not observe any significant difference among the results based on four force fields.[47] The comparison studies on different methods of deriving partial charges for computing hydration free energies of small molecules have been reported previously.[43,47,49,50] However, the systematic evaluations of the impact of different methods of deriving partial charges for predicting the protein−ligand binding free energies using the MM/PBSA and MM/GBSA approaches have rarely been reported.[44]

Here, we explored the capability of the MM/GBSA and MM/PBSA approaches to rank the binding free energies of five sets of protein−ligand systems by mixing five AMBER force fields (ff99, ff03, ff99SB, ff99SB-ILDN, and ff12SB) for proteins and four methods (RESP, ESP, AM1-BCC, and Gasteiger) of obtaining partial charges for small molecules. In order to guarantee the reliable assessment, we employed a total of 46 ligands targeted to 5 receptors with well characterized X-ray crystal structures and experimentally determined binding free energies.

MATERIALS AND METHODS

Preparation of the Tested Systems. The data set for the MM/PBSA and MM/GBSA calculations include 7 inhibitors for avidin,[13] 7 inhibitors for human thrombin,[51] 8 inhibitors for neuraminidase,[32] 16 inhibitors for Pim1 kinase, and 8 inhibitors for spleen tyrosine kinase (SYK).[52] The avidin and neuraminidase systems have also been used in our previous study.[32] The structures, experimental binding data, and PDB entries for the studied systems are listed in Table S1 of the Supporting Information. All the studied systems satisfy the following three criteria: (1) first, all the studied inhibitors have experimentally determined binding free energies, the net charges of the inhibitors are ≤1, and the inhibitors for each target show similar scaffolds; (2) second, each target at least has one crystal structure in complex with a molecule that is identical or structurally similar to the studied inhibitors, and all the investigated targets are relatively rigid with only one binding pose of the inhibitors; (3) third, all the studied targets do not contain any ion in the binding pockets, and thus the uncertainty from the inaccurate force field and PB/GB parameters for ions can be avoided effectively.

For neuraminidase, all 8 inhibitors (c1−c8) have crystal structures in complex with neuraminidase. For the other 4 systems, since the inhibitors for the same target are structurally similar, the complexes for the inhibitors involved in each of the other 4 systems were generated by manually modifying the ligand in the selected crystal structure of complex. The details for model building are described below. The complexes of the inhibitors a2−a7 for avidin were generated by manually modifying biotin

dx.doi.org/10.1021/jp404160y | J. Phys. Chem. B 2013, 117, 8408−8421

(a1) in the crystal structure of the avidin−biotin complex (PDB entry: 1avd[53]). The complexes of the inhibitors b2−b7 for human thrombin were generated by modifying the inhibitor b1 in the crystal structure of 1dwc.[54] The complexes of the inhibitors d1−d9 and d11−d16 for Pim1 kinase were generated by modifying the inhibitor d10 in the crystal structure of 3bgq[55] and a nonstandard residue at position 261 (SEP) in the crystal structure was mutated to Ala. The complexes of the inhibitors (e1−e8) for SYK were generated by modifying the inhibitor in the crystal structure of 3emg.[52] All the crystal water molecules were retained. We prepared the structures above by using SYBYL-X1.2.[56]

The studied inhibitors were optimized by semiempirical AM1 method in Gaussian 09.[57] Then, single-point calculations in Gaussian 09 were performed at HF SCF/6-31G* level on the optimized structures to derive the electrostatic potential, and the ESP and RESP partial charges were obtained from the electrostatic potential using the *antechamber* module in AMBER 12.[58] The same optimized structures were used as inputs for the *antechamber* module and used to compute the AM1-BCC charges by the *sqm* program in AMBER 12.[59] The Gasteiger charges, commonly used in some docking calculations, were derived directly from the optimized structures by *antechamber*.[58]

The general AMBER force field (*gaff*)[60] was assigned for all inhibitors in this study using *antechamber*. Five different AMBER force fields, including ff99, ff99SB, ff99SB-ILDN, ff03, and ff12SB, were assigned for the proteins, respectively. Counterions, Na^+ or Cl^-, were added to the grids that had the lowest or highest electrostatic potential to neutralize the unbalanced charges in the complexes. Each complex was immersed into a TIP3P water box[61] that extended at least 10 Å from the complex.

Molecular Dynamics (MD) Simulations. The MM minimizations and MD simulations were performed using the *sander* module in AMBER12.[62] Particle mesh Ewald (PME) was employed to handle the long-range electrostatics,[63] and an 8 Å cutoff was set to treat real-space interactions. Before the MD simulations, three minimizations were employed to relax the systems: (1) all backbone C_α atoms were restrained by the strength of 50 kcal/mol·Å^2 and the other atoms were free to move (500 cycles of steepest descent and 500 cycles of conjugate gradient minimization); (2) the strength of the restrain was decreased from 50 to 10 kcal/mol·Å^2 and the other atoms were free to move (500 cycles of steepest descent and 500 cycles of conjugate gradient minimization); (3) all atoms were optimized without any constrain (1000 cycles of steepest descent and 4000 cycles of conjugate gradient minimization).

After minimizations, each system was gradually heated from 0 to 300 K in the NVT ensemble over a period of 50 ps, and then relaxed by 50 ps MD simulations in the NPT ensemble (T = 300 K and P = 1 atm). The protein in the above two stages was restrained by the strength of 2 kcal/mol·Å^2. Finally, 4 ns NPT (T = 300 K and P = 1 atm) MD simulations were performed. Temperature was controlled by the Andersen temperature coupling scheme[64] and the pressure was controlled by the isotropic position scaling protocol applied in AMBER.[62] For each avidin complex, the MD simulations based on the ff99SB and ff03 force fields were extended to 10 ns in order to examine if longer MD simulations can improve the prediction accuracy when a force field does not perform well with short or middle time-scale MD simulations (4 ns or less). All the covalent bonds involving hydrogen atoms were constrained with the SHAKE algorithm,[65] and the time step was set to 2 fs. During the MD simulations, the atom coordinates were saved every 10 ps (100 frames/ns).

MM/PBSA and MM/GBSA Calculations. The binding free energy for each system was calculated by the MM/PBSA and MM/GBSA methodologies according to eqs 1 to 4. In the MM/GBSA and MM/PBSA calculations, the single-trajectory protocol, which is much faster than the separate-trajectory protocol with higher stability of prediction, was used.[5,25] As outlined above, the only difference between MM/PBSA and MM/GBSA is the method (PB or GB) for calculating electrostatic desolvation free energy. The gas-phase nonbonded interaction between protein and inhibitor (ΔE_{MM}) was calculated with the same force field that was used in the MD simulations. The nonpolar desolvation free energy (ΔG_{SA}) was determined by the solvent accessible surface area (SASA) based on the LCPO algorithm:[66] ΔG_{SA}= 0.0072 × ΔSASA.

In the MM/GBSA calculations, the polar desolvation free energy was calculated by the modified GB model developed by Onufriev and co-workers (GB^{OBC1}).[29] According to our previous study, GB^{OBC1} performs better than the other two GB models (GB^{HCT} and GB^{OBC2}) in AMBER,[32] and therefore, the GB^{OBC1} model was employed in this study. In the PB and GB calculations the exterior dielectric constant (solvent) was set to 80 and the interior dielectric constant (solute) was set to 1, 2, or 4.

In the MM/PBSA calculations, the polar desolvation free energy was calculated by the PB solver implemented in the *pbsa* module in AMBER12.[67,68] The radii optimized by Tan and Luo with respect to the reaction field energies computed in the TIP3P explicit solvents were used.[69] The partial charges used in the PB calculations were taken from the force field parameter set for protein and the partial charges for inhibitor. The grid size was defined as 0.5 Å. Due to the expensive computational demand and no apparent improvement in most cases, entropies were not considered here.[16,18,46,48] Thus, in this study, only the enthalpies were used for comparison.

Estimation Methods. The Pearson coefficient (r_p) was employed to evaluate the linear correlation between the predicted binding free energies and the experimental data, and the Spearman ranking coefficient (r_s) was employed to evaluate the capability of MM/GBSA or MM/PBSA to rank binding free energies. It is well-known that MM/PBSA or MM/GBSA is usually used to rank the binding affinities for most systems rather than give accurate predictions of the absolute binding free energies.[32] Therefore, the Spearman correlation coefficient is a better choice to evaluate MM/GBSA or MM/PBSA for ranking the binding affinities. In order to give an overall estimation of the impact of different force fields and partial charge models on the predictions for different systems, the Spearman correlation coefficients for the five systems was simply summed up and defined as "ranking score".

RESULTS AND DISCUSSION

Effect of the Force Field on the Performance of MM/GBSA. We first compared the performance of MM/GBSA with five different force fields available in AMBER12 to rank the binding free energies. The binding free energies predicted by MM/GBSA with different force fields are summarized in Table 1. The energy terms were averaged over the snapshots extracted from 4 ns MD trajectories. The RESP partial charges were used for the MM/PBSA and MM/GBSA calculations.

As shown in Table 1, for avidin, all of the tested force fields perform well. The Spearman correlation coefficient r_s ranges from 0.89 (ff99, ff99SB, and ff99SB-ILDN) to 1.0 (ff03 and ff12SB).

dx.doi.org/10.1021/jp404160y | J. Phys. Chem. B 2013, 117, 8408−8421

Table 1. The Highest Spearman and Pearson Correlation Coefficients (r_s and r_p) and the Corresponding Solute Dielectric Constants for the MM/GBSA Calculations with Five AMBER Force Fields Based on the 0.2−4 ns MD Trajectories[a]

	ff99		ff03		ff99SB		ff99SB-ILDN		ff12SB	
	r_s[a]	r_p[b]	r_s	r_p	r_s	r_p	r_s	r_p	r_s	r_p
avidin	ε_{in} = 1	ε_{in} = 1	ε_{in} = 1	ε_{in} = 1	ε_{in} = 1	ε_{in} = 1	ε_{in} = 1	ε_{in} = 1	ε_{in} = 1	ε_{in} = 1
	0.89	0.82	1.00	0.92	0.89	0.84	0.89	0.90	1.00	0.92
human thrombin	ε_{in} = 2	ε_{in} = 2	ε_{in} = 2	ε_{in} = 2	ε_{in} = 4	ε_{in} = 4	ε_{in} = 4	ε_{in} = 2	ε_{in} = 1	ε_{in} = 2
	0.96	0.99	0.75	0.62	0.57	0.64	0.07	0.52	0.50	0.55
neuraminidase	ε_{in} = 4	ε_{in} = 4	ε_{in} = 4	ε_{in} = 4	ε_{in} = 4	ε_{in} = 4	ε_{in} = 4	ε_{in} = 4	ε_{in} = 4	ε_{in} = 4
	0.43	0.41	0.02	0.17	0.36	0.18	0.37	0.21	0.4	0.4
Pim-1 kinase	ε_{in} = 2	ε_{in} = 2	ε_{in} = 1	ε_{in} = 1	ε_{in} = 1	ε_{in} = 2	ε_{in} = 1	ε_{in} = 1	ε_{in} = 1	ε_{in} = 1
	0.56	0.5	0.62	0.62	0.72	0.73	0.74	0.74	0.58	0.59
SYK	ε_{in} = 2	ε_{in} = 4	ε_{in} = 1	ε_{in} = 1	ε_{in} = 4	ε_{in} = 4	ε_{in} = 4	ε_{in} = 4	ε_{in} = 2	ε_{in} = 1
	0.63	0.35	0.63	0.57	0.40	0.19	−0.14	−0.11	0.34	0.56
ranking score	3.47		3.02		2.94		1.93		2.82	

[a]The values of [a]r_s and [b]r_p in the Tables 1 and 3−7, are all the highest Spearman and Pearson correlation coefficients among the three dielectric constants (1, 2, and 4) under different calculation process.

Our results are consistent with the observations reported by Weis and co-workers.[47] Weis et al. compared the impact of four AMBER force fields on the binding free energies predicted by MM/GBSA for seven avidin inhibitors, and they did not find any significant difference between ff94, ff99, and ff03. The avidin inhibitors are well ranked and the reason is that, as previously analyzed,[32,47] the range of the binding free energies of the studied inhibitors is quite large, from −4.5 kcal/mol to −20.4 kcal/mol. However, for the other four receptor systems, large differences in the MM/GBSA predictions with different force fields for inhibitor ranking were observed.

For human thrombin, as shown in Figure 1 B1, the ff99 force field performs especially well with r_s = 0.96 and r_p = 0.99, which are substantially better than the other force fields (r_s = 0.07−0.75 and r_p = 0.38−0.75). For Pim1, the Spearman correlation coefficient r_s ranges from 0.56 (ff99) to 0.74 (ff99SB-ILDN). Both of the ff99SB and ff99SB-ILDN force fields show relatively good performance (r_s = 0.72 and 0.74).

For SYK, a large difference of r_s was observed among different force fields with the best r_s of 0.63 (ff03 and ff99) and the worst r_s of −0.14 (ff99SB-ILDN). That is to say, the ff99SB-ILDN force field even gives a reverse prediction for the studied inhibitors, indicating that the force field used in simulations should be chosen carefully.

The performance of MM/GBSA for neuraminidase is the worst, and the best r_s is 0.43 (ff99). This suggests that all the force fields failed in ranking the binding affinities of the neuraminidase inhibitors. The poor prediction of the neuraminidase inhibitors is caused by the strong electrostatic interactions between the inhibitors and the binding pocket, which impedes the accurate estimation of the polar desolvation free energies, as discussed in our previous study.[32]

In order to evaluate the overall ranking capabilities for the five force fields, we simply summed up the Spearman correlation coefficient r_s, and took it as a ranking score for evaluating different force fields. The results show that the ff99 force field gives the best performance with a ranking score of 3.47, whereas the ff99SB-ILDN force field gives the worst prediction with a ranking score of only 1.93. Obviously, the ff99 force field should be employed in most cases when no precedents can be learned. However, the ff99SB-ILDN force field still may be successfully used in some systems that have been well tested. For example, MM/GBSA with the ff99SB-ILDN force field shows the best capability to rank the inhibitors of Pim1 kinase, with r_s =0.74 and r_p = 0.74 (Figure 1 D4).

Similar to the previous studies,[32] several solute dielectric constants (ε_{in} = 1, 2, or 4) were employed in the GB calculations. As listed in Table 1, the predictions are quite sensitive to the dielectric constant. For avidin, ε_{in} = 1 gives the highest Spearman correlation coefficients for all five force fields, and ε_{in} = 4 (or higher) may give reasonable predictions for neuraminidase due to the highly polarized binding pockets. However, for the other three systems, the best dielectric constant with the highest Spearman correlation coefficient is different for various force fields. For example, for human thrombin, ε_{in} = 2 gives the best predictions for the ff99 and ff03 force fields, ε_{in} = 4 gives the best predictions for the ff99SB and ff99SB-ILDN force fields, and ε_{in} = 1 gives the best performance for the ff12SB force field.

A deep analysis of the energy components (Table 2) for the human thrombin inhibitors shows that the nonpolar interactions ($\Delta E_{vdW}+\Delta G_{SA}$) are stable while the polar interactions ($\Delta E_{elec}+\Delta G_{GB}$) have relatively large fluctuations. Especially, for the inhibitors b5 and b6, the fluctuation is even larger than the polar interactions themselves. That is to say, the polar interactions are not as stable as the nonpolar interactions. Therefore, choosing the best solute dielectric constant is essential for accurate predictions of binding free energy, since it can scale the electrostatic interactions. For the inhibitors with small difference of binding free energies, for example, the 16 Pim1 kinase inhibitors with ΔG = −7.8 to −10.9 kcal/mol and the 8 SYK inhibitors with ΔG = −7.8 to −11 kcal/mol (Table S1 in the Supporting Information), slight fluctuations of the polar interactions may affect the ranking results significantly. Moreover, by comparing Tables 1 and 3 (the results based on 1 ns MD simulations and will be discussed in the next section), we observe that the best dielectric constants judged by the predicted binding affinities based on different lengths of MD simulations may be different. For example, for human thrombin, ε_{in} = 1 seems the best choice for the ff99 force field, but ε_{in} = 2 shows better ranking performance when the MD simulations going on. Therefore, for some systems, rigorous validation is necessary for choosing a reliable dielectric constant.

Can Relatively Longer MD Simulations Improve the Predictions? Our previous studies show that short MD simulations may give a better performance for ranking binding free energy (only studied by the ff03 force field)[32] than longer MD simulations, and thus here we analyzed the results based on

dx.doi.org/10.1021/jp404160y | J. Phys. Chem. B 2013, 117, 8408−8421

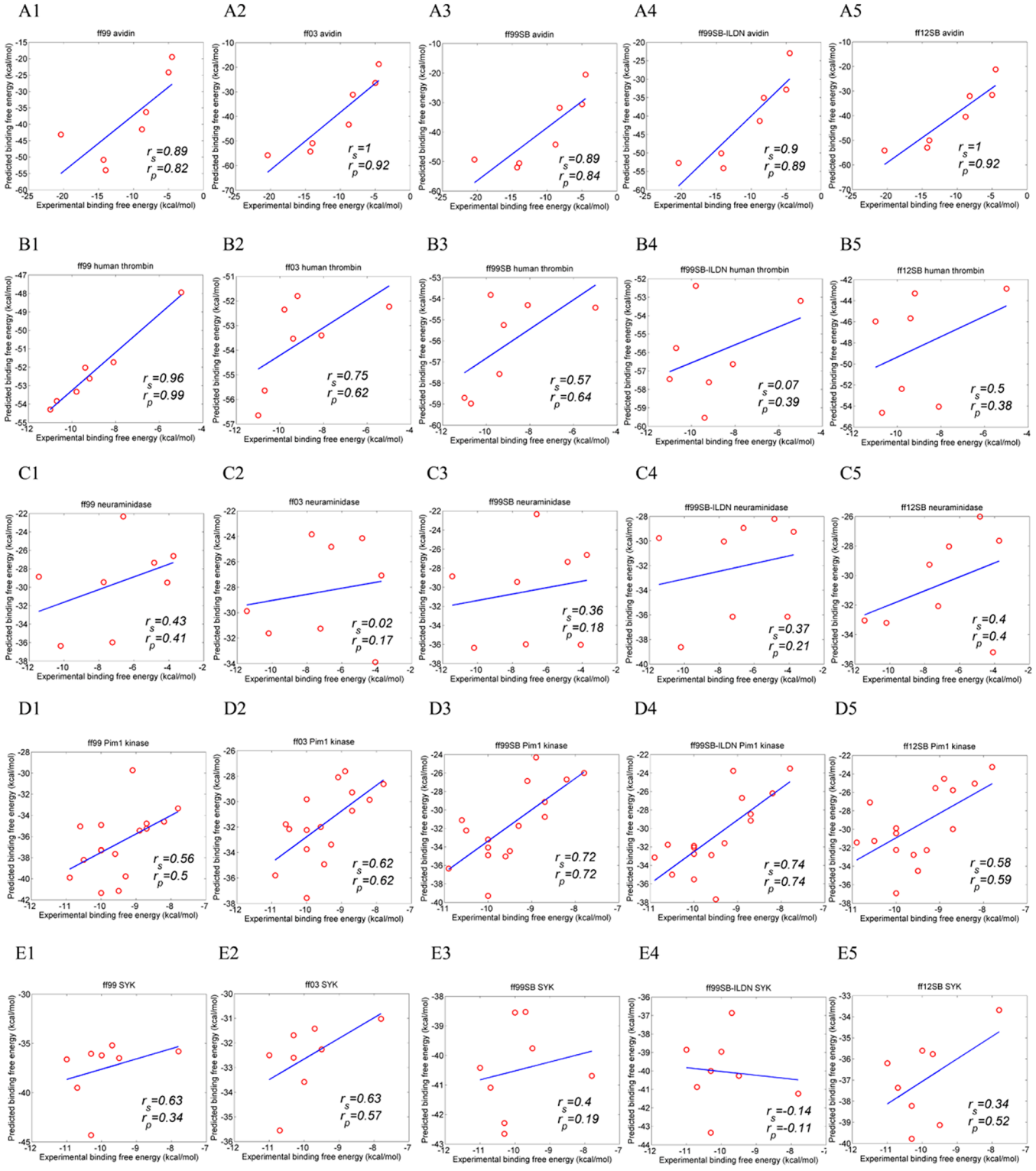

Figure 1. Spearman and Pearson correlations (r_s and r_p) between the binding free energies calculated by MM/GBSA based on the 4 ns MD trajectories and the experimental values for (A) avidin, (B) human thrombin, (C) neuraminidase, (D) Pim1 kinase, and (E) SYK with the five AMBER force fields, including (1) ff99, (2) ff03, (3) ff99SB, (4) ff99SB-ILDN, and (5) ff12SB.

the 0.2−1 ns MD trajectories. As shown in Table 3, for the ff03 force field, the results based on the 0.2−1 ns MD trajectories are a bit better than those based on 0.2−4 ns MD trajectories (Table 1), with the ranking scores of 3.25 versus 3.02. In addition, the ff99SB-ILDN force field also shows better performance when the calculations were based on 0.2−1 ns instead of 0.2−4 ns MD trajectories. However, for the other three force fields (ff99, ff99SB, and ff12SB), the short time-scale MD simulations give slightly worse performance than the longer MD simulations, with the ranking scores of 3.24 versus 3.47 for the ff99 force field, 2.92 versus 2.94 for the ff99SB force field, and 2.68 versus 2.82 for the ff12SB force field.

dx.doi.org/10.1021/jp404160y | J. Phys. Chem. B 2013, 117, 8408−8421

Table 2. Comparison of the Calculated Effective Binding Free Energies (Enthalpies, $\Delta E_{enthalpy}$) of the Human Thrombin System Based on Five Force Fields with the Dielectric Constant of 1 and the Simulation Time of 4 ns (kcal/mol)

		b1	b2	b3	b4	b5	b6	b7
ff99	$\Delta E_{elec} + \Delta G_{GB}$ [a]	13.56 ± 0.86[c]	12.16 ± 0.42	15.82 ± 1.82	13.15 ± 0.86	2.23 ± 1.22	0.01 ± 0.43	13.53 ± 0.98
	$\Delta E_{vdW} + \Delta G_{SA}$ [b]	−60.46 ± 0.44	−57.30 ± 0.03	−55.38 ± 0.18	−58.58 ± 0.15	−53.96 ± 0.71	−52.36 ± 1.11	−58.14 ± 0.67
	$\Delta E_{enthalpy}$	−46.90 ± 0.42	−45.15 ± 0.45	−35.99 ± 2.00	−45.42 ± 0.71	−51.73 ± 1.93	−52.35 ± 1.54	−44.61 ± 0.31
ff03	$\Delta E_{elec} + \Delta G_{GB}$	12.82 ± 0.81	12.12 ± 0.47	9.15 ± 2.35	13.62 ± 1.89	4.02 ± 0.4	0.67 ± 1.14	14.14 ± 0.17
	$\Delta E_{vdW} + \Delta G_{SA}$	−62.45 ± 0.48	−58.76 ± 0.00	−55.95 ± 0.33	−57.59 ± 1.6	−56.64 ± 0.94	−51.81 ± 0.49	−60.23 ± 1.05
	$\Delta E_{enthalpy}$	−49.63 ± 1.3	−46.64 ± 0.47	−46.80 ± 2.68	−43.98 ± 0.29	−52.62 ± 0.55	−51.14 ± 0.66	−46.09 ± 0.87
ff99SB	$\Delta E_{elec} + \Delta G_{GB}$	14.41 ± 0.85	9.37 ± 0.81	2.10 ± 0.76	10.21 ± 1.65	9.72 ± 0.14	6.98 ± 1.52	11.86 ± 0.21
	$\Delta E_{vdW} + \Delta G_{SA}$	−61.41 ± 0.27	−55.83 ± 0.23	−54.04 ± 1.01	−56.85 ± 0.51	−59.88 ± 0.16	−54.12 ± 0.50	−59.53 ± 0.70
	$\Delta E_{enthalpy}$	−46.99 ± 0.58	−46.45 ± 1.03	−51.94 ± 0.25	−46.64 ± 1.14	−50.16 ± 0.02	−47.14 ± 1.02	−47.67 ± 0.49
ff99SB-ILDN	$\Delta E_{elec} + \Delta G_{GB}$	15.39 ± 1.00	2.85 ± 2.23	15.54 ± 1.78	12.13 ± 0.55	9.38 ± 1.99	−2.82 ± 1.88	11.30 ± 1.72
	$\Delta E_{vdW} + \Delta G_{SA}$	−60.37 ± 0.15	−56.40 ± 0.11	−56.36 ± 0.20	−59.66 ± 0.05	−56.51 ± 0.43	−50.19 ± 0.65	−61.35 ± 1.00
	$\Delta E_{enthalpy}$	−44.99 ± 1.15	−53.55 ± 2.34	−40.83 ± 1.98	−47.54 ± 0.60	−47.13 ± 1.55	−53.02 ± 1.23	−50.05 ± 0.71
ff12SB	$\Delta E_{elec} + \Delta G_{GB}$	14.41 ± 1.91	2.79 ± 0.58	12.03 ± 0.00	13.92 ± 1.65	−2.50 ± 0.33	−1.86 ± 0.15	13.86 ± 0.76
	$\Delta E_{vdW} + \Delta G_{SA}$	−60.37 ± 0.00	−56.85 ± 2.96	−54.88 ± 0.84	−57.22 ± 0.98	−52.12 ± 0.60	−50.49 ± 0.92	−59.54 ± 0.02
	$\Delta E_{enthalpy}$	−45.96 ± 1.91	−54.05 ± 3.54	−42.86 ± 0.84	−43.30 ± 2.63	−54.62 ± 0.27	−52.35 ± 0.77	−45.67 ± 0.75
average	$\Delta E_{elec} + \Delta G_{GB}$	14.23 ± 0.80	7.85 ± 4.72	10.83 ± 5.69	12.26 ± 1.41	4.61 ± 5.13	1.10 ± 4.01	13.05 ± 1.43
	$\Delta E_{vdW} + \Delta G_{SA}$	−61.07 ± 1.03	57.07 ± 1.19	−55.35 ± 0.93	−57.90 ± 1.19	−55.86 ± 2.96	−52.05 ± 1.68	−59.77 ± 1.18
	$\Delta E_{enthalpy}$	−46.84 ± 1.62	−49.22 ± 4.24	−44.52 ± 5.11	−45.64 ± 1.60	−51.25 ± 2.81	−50.95 ± 2.44	−46.72 ± 2.17
	ΔG_{exp}	−11	−8.1	−5	−9.2	−10.7	−9.8	−9.4

[a] $\Delta E_{elec} + \Delta G_{GB}$ denotes polar part of the enthalpy ($\Delta E_{enthalpy}$). [b] $\Delta E_{vdW} + \Delta G_{SA}$ represents the nonpolar part of the enthalpy. [c] The statistical error was estimated on the basis of the deviation between two block averages.

Table 3. Highest Spearman and Pearson Correlation Coefficients (r_s and r_p) and the Corresponding Solute Dielectric Constants for the MM/GBSA Calculations with Five AMBER Force Fields Based on the 0.2−1 ns MD Trajectories

	ff99		ff03		ff99SB		ff99SB-ILDN		ff12SB	
	r_s	r_p	r_s	r_p	r_s	r_p	r_s	r_p	r_s	r_p
avidin	ε_{in} = 1	ε_{in} = 1	ε_{in} = 1	ε_{in} = 1	ε_{in} = 1	ε_{in} = 1	ε_{in} = 1	ε_{in} = 1	ε_{in} = 1	ε_{in} = 1
	0.86	0.76	1	0.91	0.89	0.86	0.86	0.82	0.96	0.87
human thrombin	ε_{in} = 1	ε_{in} = 1	ε_{in} = 1	ε_{in} = 1	ε_{in} = 4	ε_{in} = 4	ε_{in} = 1	ε_{in} = 2	ε_{in} = 2	ε_{in} = 2
	0.86	0.94	0.93	0.83	0.5	0.4	0.39	0.54	0.71	0.76
neuraminidase	ε_{in} = 4	ε_{in} = 4	ε_{in} = 4	ε_{in} = 4	ε_{in} = 4	ε_{in} = 4	ε_{in} = 4	ε_{in} = 4	ε_{in} = 4	ε_{in} = 4
	0.57	0.47	0.12	0.44	0.21	0.23	0.24	0.48	0.1	0
Pim-1 kinase	ε_{in} = 1	ε_{in} = 1	ε_{in} = 4	ε_{in} = 2	ε_{in} = 1	ε_{in} = 4	ε_{in} = 1	ε_{in} = 1	ε_{in} = 1	ε_{in} = 1
	0.67	0.62	0.67	0.67	0.7	0.75	0.72	0.75	0.61	0.66
SYK	ε_{in} = 2	ε_{in} = 2	ε_{in} = 4	ε_{in} = 2	ε_{in} = 1	ε_{in} = 1	ε_{in} = 4	ε_{in} = 4	ε_{in} = 4	ε_{in} = 4
	0.28	0.18	0.53	0.57	0.62	0.29	0.1	0.07	0.3	0.24
ranking score	3.24		3.25		2.92		2.31		2.68	

In order to investigate the time dependence of the ranking capabilities for different force fields, the time evolution curves of the Spearman correlation coefficients were plotted (Figure 2). For ff03 (blue curve), the Spearman correlation coefficients decline for neuraminidase and Pim1 kinase, remain stable for avidin and human thrombin, and increase for SYK. For most systems the shorter MD simulations based on the ff03 force field give better ranking results than the prolonged simulations.

However, shorter MD simulations may not be the best choice for the other force fields. For ff99 (red curve), the Spearman correlation coefficients for three systems (avidin, human thrombin, and SYK) increase along the simulations, and those for Pim1 kinase and neuraminidase rise at the first 2 ns and then decline. For the ff99SB (cyan curve), the Spearman correlation coefficients rise for three systems (human thrombin, neuraminidase, and Pim1 kinase), remains stable for avidin, and decrease for SYK. For ff99SB-ILDN (purple curve), the Spearman correlation coefficients rise for avidin, decline for human thrombin and SYK, rise at the first 2 and 3 ns, and then decline for neuraminidase and Pim1 kinase, respectively. For ff12SB (green curve), the Spearman correlation coefficients rise for avidin and neuraminidase, rise at the first 2 ns and then decline for human thrombin, and decline at the first 2 ns and then rise for Pim1 kinase. Interestingly, the Spearman correlation coefficients for SYK show significant fluctuation, and it is possible that the ff12SB force field cannot give stable simulations for the SYK systems. Therefore, reasonably longer MD simulations will be helpful for achieving stable predictions for the ff99, ff99SB, ff99SB-ILDN, and ff12SB force fields, but shorter MD simulations are preferred for the ff03 force field.

The previous discussions are based on middle time-scale simulations (4 ns), and it is concluded that the shorter simulations (1 ns) will be enough for the ff03 force field. However, no tests have been preformed for the relatively longer MD simulations (10 ns). Here, 10 ns MD simulations were performed for the avidin inhibitors. Due to the expensive computational demand, only the ff03 and ff99SB force fields were employed for the avidin systems. As illustrated in Figure 2F, for these two force fields, the

dx.doi.org/10.1021/jp404160y | J. Phys. Chem. B 2013, 117, 8408−8421

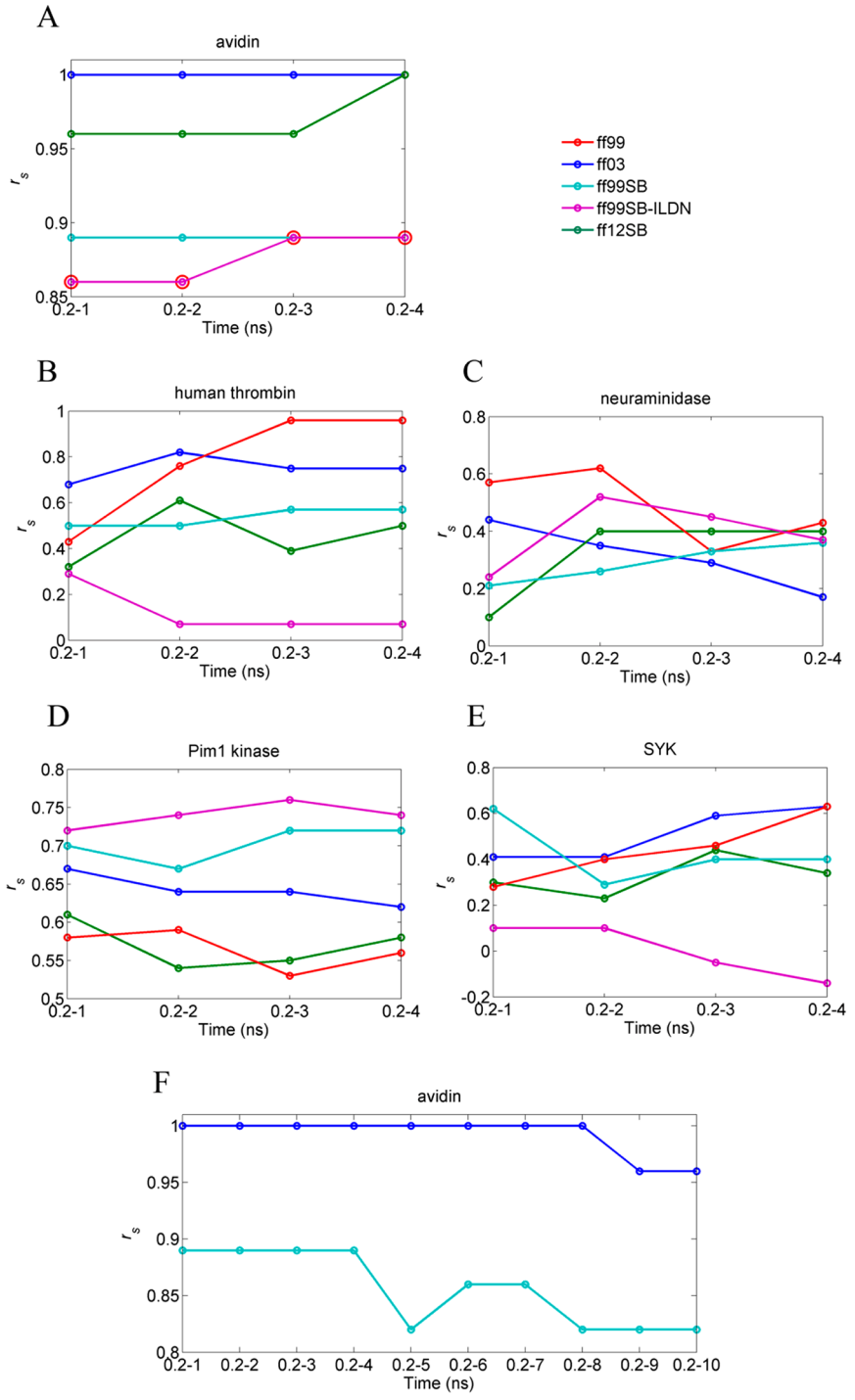

Figure 2. The time evolution of the Spearman correlations (r_s) calculated by MM/GBSA based on the 4 ns (A–E) and 10 ns MD trajectories (F) for (A) avidin, (B) human thrombin, (C) neuraminidase, (D) Pim1 kinase, and (E) SYK with the five AMBER force fields, including (1) ff99 (red), (2) ff03 (blue), (3) ff99SB (cyan), (4) ff99SB-ILDN, and (5) ff12SB.

Spearman correlation coefficients are stable originally and then decrease along the simulations; that is to say, if the ranking results cannot be improved at the beginning of the simulations, such as the first 4 ns, the longer the simulations are performed, the worse the results obtained. It is possible that with the simulation time extended, the protein complexes for some inhibitors may undergo large conformational changes due to inaccurate force field parameters, which may result in different binding modes of inhibitors compared with those in the crystal structures. As shown in Figure 3, for the AMBER03 force field, except inhibitors a2 (green) and a3 (red), most avidin complexes show increased and fluctuated root-mean-square deviations (RMSDs) at the later stage of the MD simulations. Therefore, a reasonable time scale of MD simulations, such as 1–4 ns, will be enough for most cases when calculating binding free energies based on well-characterized X-ray crystal structures. However, further studies may still be needed to determine whether much longer simulations, such as microsecond-level MD simulations, should be used for the systems with flexible binding sites.

dx.doi.org/10.1021/jp404160y | J. Phys. Chem. B 2013, 117, 8408–8421

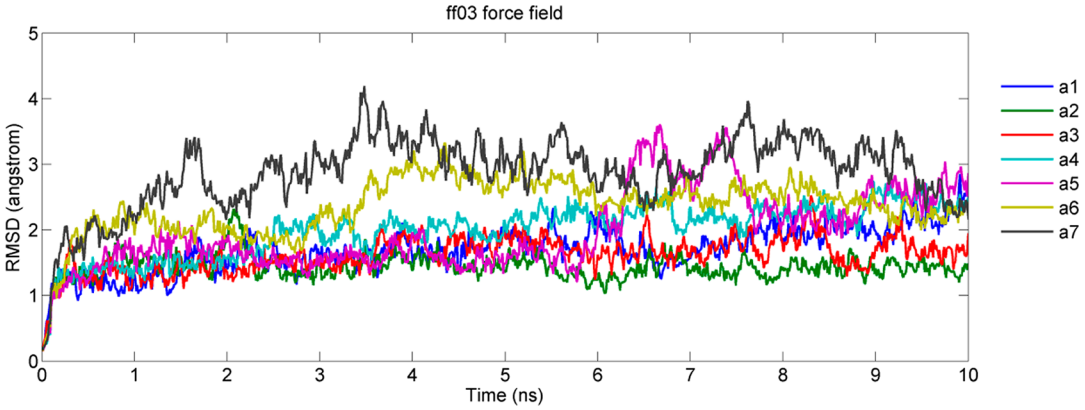

Figure 3. Root-mean-square deviations (RMSDs) of the backbone of the avidin systems based on the 10 ns trajectories simulated by the ff03 force field.

Comparison of the Ranking Results by MM/GBSA (GB^{OBC1}) and MM/PBSA. In our previous study,[32] we compared the performance of MM/GBSA with three GB models (GB^{HTC}, GB^{OBC1}, and GB^{OBC2}) and MM/PBSA with the Delphi II program,[70] and we found that MM/GBSA with GB^{OBC1} achieves the best performance, even better than MM/PBSA with Delphi II. In AMBER12, the default PB solver is implemented in the *pbsa* program developed by Lu and Luo.[68] Moreover, the compatible radii for *pbsa* were optimized by Tan and Luo with respect to the reaction field energies computed in the TIP3P explicit solvents,[69] which were not tested in our previous studies.[32] Therefore, it is possible that the *pbsa* program has better compatibility with the AMBER force field than Delphi II. Thus, in this section, we compared the performance of MM/GBSA with GB^{OBC1} and MM/PBSA with *pbsa* and Tan's radii set for three most popular AMBER force fields (ff99, ff03, and ff99SB) based on 4 ns MD simulations. As listed in Table 4, the ranking scores for the ff03 and ff99SB force fields based on MM/PBSA (3.38 and 3.51) are obviously higher than those based on MM/GBSA (3.02 and 2.94) as shown in Table 1. For ff99, the ranking score of MM/PBSA is 3.13, which is worse than that of MM/GBSA (3.47).

Table 4. Highest Spearman and Pearson Correlation Coefficients (r_s and r_p) and the Corresponding Solute Dielectric Constants for the MM/PBSA Calculations with Three AMBER Force Fields Based on the 0.2−4 ns MD Trajectories

	ff99		ff03		ff99SB	
	r_s	r_p	r_s	r_p	r_s	r_p
avidin	ε_{in} = 1	ε_{in} = 1	ε_{in} = 1	ε_{in} = 1	ε_{in} = 1	ε_{in} = 1
	0.89	0.82	1	0.95	0.89	0.89
human thrombin	ε_{in} = 2	ε_{in} = 4	ε_{in} = 4	ε_{in} = 2	ε_{in} = 4	ε_{in} = 4
	0.79	0.95	0.75	0.61	0.86	0.71
neuraminidase	ε_{in} = 4	ε_{in} = 4	ε_{in} = 4	ε_{in} = 4	ε_{in} = 4	ε_{in} = 4
	0.31	0.50	0.49	0.48	0.19	0.2
Pim-1 kinase	ε_{in} = 1	ε_{in} = 1	ε_{in} = 2	ε_{in} = 2	ε_{in} = 1	ε_{in} = 1
	0.65	0.58	0.59	0.61	0.74	0.76
SYK	ε_{in} = 4	ε_{in} = 4	ε_{in} = 2	ε_{in} = 1	ε_{in} = 1	ε_{in} = 1
	0.49	0.34	0.55	0.70	0.83	0.75
ranking score	3.13		3.38		3.51	

Further investigations show that MM/PBSA with the ff03 force field (r_s = 0.49) gives much better performance than MM/GBSA with the ff03 force field (0.02) to rank the neuraminidase inhibitors. However, for Pim1 kinase and SYK, the predictions given by MM/PBSA with the ff03 force field become slightly worse than those given by MM/GBSA with the ff03 force field (Figure 4D). For the ff99SB force field, as illustrated in Figure 4F, the ranks predicted by MM/PBSA for human thrombin and SYK are remarkably improved, indicated by the r_s values of 0.86 and 0.83, compared to those of 0.57 and 0.40 given by MM/GBSA.

For the ff99SB force field, MM/PBSA gives a worse prediction (r_s = 0.19), indicating that MM/PBSA cannot rank the neuraminidase inhibitors effectively. Moreover, for the ff99 force field, the predictions given by MM/PBSA are worse than those by MM/GBSA (GB^{OBC1}) for several systems, including human thrombin, neuraminidase, and SYK. However, overall, for most cases, MM/PBSA with the *pbsa* program gives better predictions than MM/GBSA (GB^{OBC1}).

The MM/PBSA results with three force fields (ff99, ff99SB, and ff03) were compared. As shown in Table 4, the ff99SB force field shows satisfactory performance for four systems, including avidin (r_s = 0.89), human thrombin (r_s = 0.86), Pim1 kinase (r_s = 0.74), and SYK (r_s = 0.83), but it does not give acceptable predictions for neuraminidase (r_s = 0.49).

In fact, as shown in Figure 4 (B, D, F), no force field, based on either MM/PBSA or MM/GBSA with the MD simulations of 4 ns, gives reasonable predictions for the neuraminidase systems, and even r_s for the best prediction given by MM/PBSA based on the ff03 force field is slightly below 0.5 (0.49). That is to say, all force fields

Table 5. Highest Spearman and Pearson Correlation Coefficients (r_s and r_p) and the Corresponding Solute Dielectric Constants for the MM/PBSA Calculations with Three AMBER Force Fields Based on the 0.2−1 ns MD Trajectories

	ff99		ff03		ff99SB	
	r_s	r_p	r_s	r_p	r_s	r_p
avidin	ε_{in} = 1	ε_{in} = 1	ε_{in} = 1	ε_{in} = 1	ε_{in} = 1	ε_{in} = 1
	0.86	0.75	1.00	0.95	0.89	0.89
human thrombin	ε_{in} = 2	ε_{in} = 2	ε_{in} = 2	ε_{in} = 2	ε_{in} = 4	ε_{in} = 4
	0.86	0.89	0.79	0.77	0.5	0.53
neuraminidase	ε_{in} = 4	ε_{in} = 4	ε_{in} = 4	ε_{in} = 4	ε_{in} = 4	ε_{in} = 4
	0.55	0.52	0.69	0.72	0.29	0.29
Pim-1 kinase	ε_{in} = 1	ε_{in} = 1	ε_{in} = 2	ε_{in} = 2	ε_{in} = 2	ε_{in} = 4
	0.63	0.61	0.66	0.66	0.70	0.75
SYK	ε_{in} = 4	ε_{in} = 4	ε_{in} = 2	ε_{in} = 4	ε_{in} = 1	ε_{in} = 1
	0.32	0.18	0.55	0.52	0.86	0.68
ranking score	3.22		3.69		3.24	

dx.doi.org/10.1021/jp404160y | J. Phys. Chem. B 2013, 117, 8408−8421

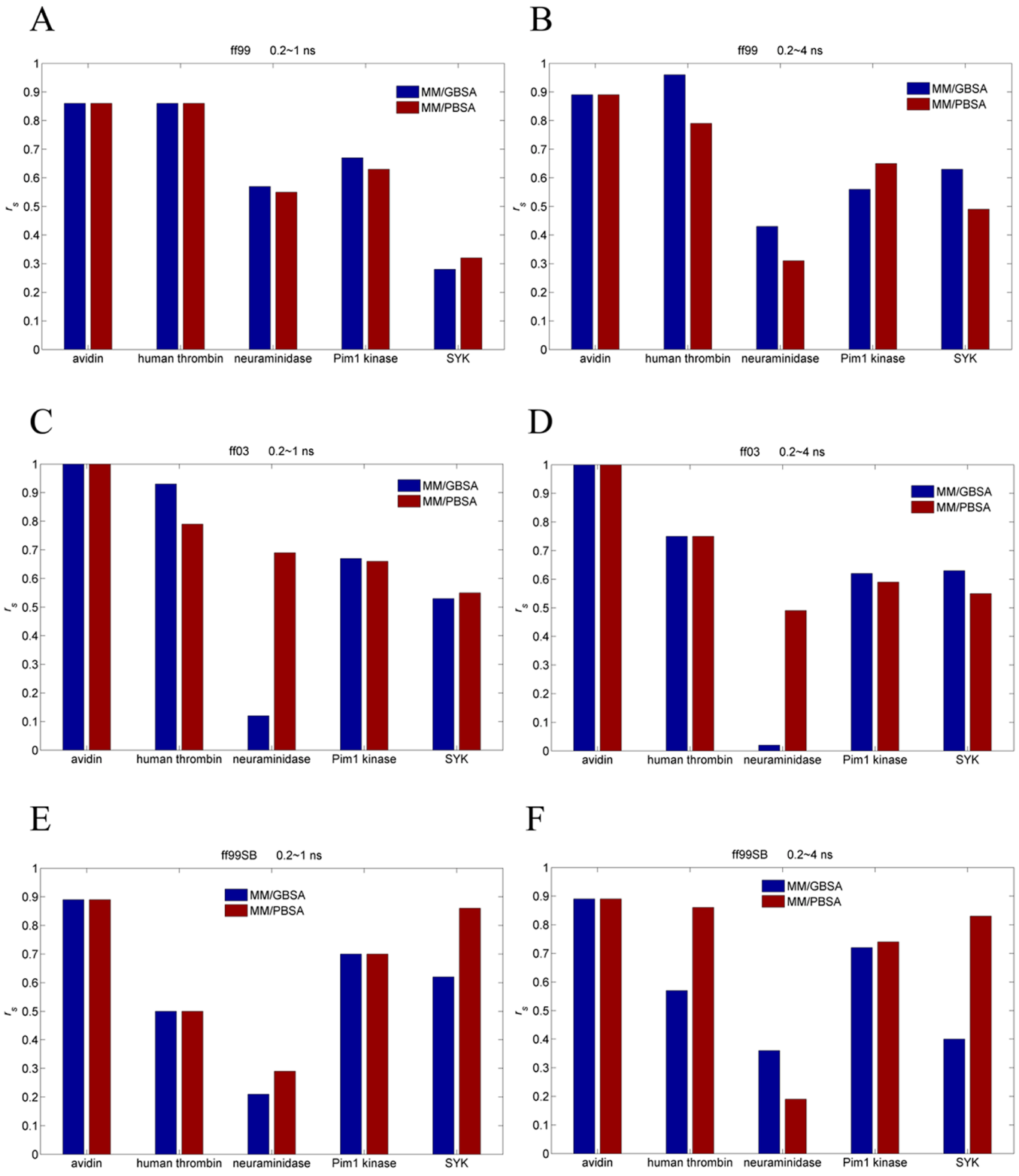

Figure 4. The comparison of MM/GBSA (blue) and MM/PBSA (red) results of five systems and three force fields based on 1 and 4 ns simulation trajectories. (A) ff99 based on the 1 ns simulations, (B) ff99 based on the 4 ns simulations, (C) ff03 based on the 1 ns simulations, (D) ff03 based on the 4 ns simulations, (E) ff99SB based on the 1 ns simulations, and (F) ff99SB based on the 4 ns simulations.

fail in ranking the binding affinities for the neuraminidase systems. Thus, for most cases, the ff99SB force field is a good choice for MM/PBSA based on a reasonable time scale of MD simulations (4 ns).

Then, the MM/PBSA results between short time-scale (0.2−1 ns) and middle time-scale simulations (0.2−4 ns) were also compared. As shown in Table 4, Table 5, and Figure 4, the ff03 force field performs better with the ranking score of 3.69 than the other two force fields, and even the r_s of neuraminidase also reaches to 0.69. Therefore, for the MM/PBSA calculations based on shorter MD simulations (1 ns), the ff03 force field is also a good choice.

dx.doi.org/10.1021/jp404160y | J. Phys. Chem. B 2013, 117, 8408−8421

Table 6. Highest Spearman and Pearson Correlation Coefficients (r_s and r_p) and the Corresponding Solute Dielectric Constants for the MM/GBSA Calculations with Different Partial Charges for Ligands Based on the 0.2−1 ns MD Trajectories

	RESP		AM1-BCC		ESP		GAS	
	r_s	r_p	r_s	r_p	r_s	r_p	r_s	r_p
avidin	ε_{in} = 1	ε_{in} = 1	ε_{in} = 1	ε_{in} = 1	ε_{in} = 1	ε_{in} = 1	ε_{in} = 1	ε_{in} = 1
	1.00	0.91	0.89	0.88	0.96	0.93	0.21	0.62
human thrombin	ε_{in} = 1	ε_{in} = 1	ε_{in} = 1	ε_{in} = 1	ε_{in} = 4	ε_{in} = 2	ε_{in} = 4	ε_{in} = 2
	0.93	0.83	0.57	0.49	0.46	0.39	0.36	0.30
neuraminidase	ε_{in} = 4	ε_{in} = 4	ε_{in} = 4	ε_{in} = 4	ε_{in} = 4	ε_{in} = 4	ε_{in} = 4	ε_{in} = 4
	0.12	0.44	0.40	0.44	0.33	0.29	0.14	−0.01
Pim-1 kinase	ε_{in} = 4	ε_{in} = 2	ε_{in} = 1	ε_{in} = 1	ε_{in} = 1	ε_{in} = 1	ε_{in} = 1	ε_{in} = 2
	0.67	0.67	0.66	0.72	0.69	0.69	0.63	0.57
SYK	ε_{in} = 4	ε_{in} = 2	ε_{in} = 1	ε_{in} = 2	ε_{in} = 2	ε_{in} = 1	ε_{in} = 1	ε_{in} = 2
	0.53	0.57	0.57	0.22	0.74	0.65	0.51	0.74
ranking score	3.25		3.09		3.18		1.85	

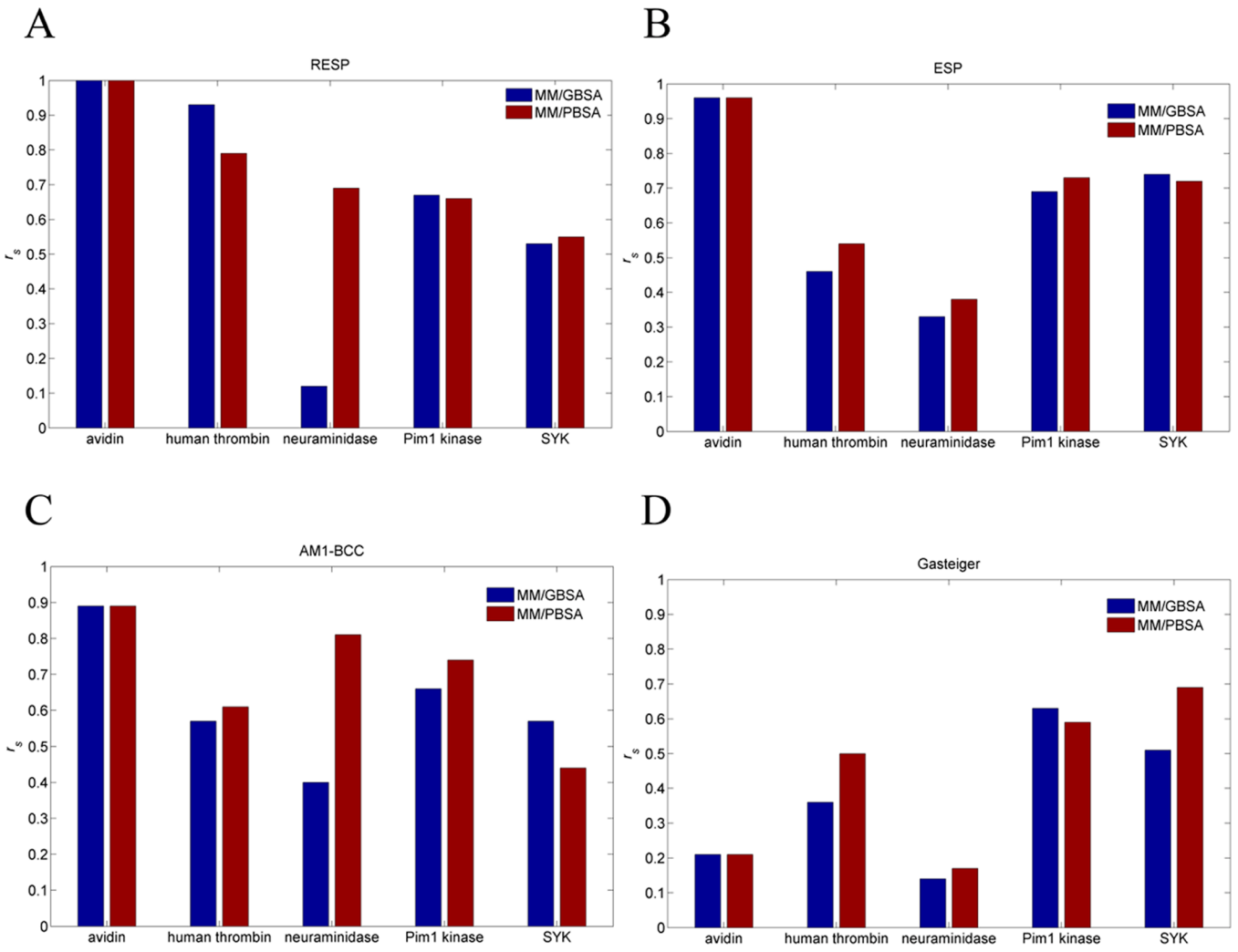

Figure 5. Comparison of the MM/GBSA (blue) and MM/PBSA (red) results based on the 1 ns simulations for (A) the RESP charges, (B) the ESP charges, (C) the AM1-BCC charges, and (D) the Gasteiger charges.

In summary, for the ff03 and ff99SB force fields, the binding free energies calculated by MM/PBSA with the *pbsa* program give better ranking results than those calculated by MM/GBSA with GB^{OBC1}. Moreover, for most cases, short and middle time-scale MD simulations are compatible with the ff03 and ff99SB force fields, respectively.

Effect of Ligand Charge Models on MM/GBSA and MM/PBSA. Since the ff03 force field performs well in ranking inhibitors based on shorter MD simulations, we employed it to examine how the methods of obtaining partial charges for ligands, including the RESP, ESP, AM1-BCC, and Gasteiger charges, affect the ranking results given by MM/GBSA and

dx.doi.org/10.1021/jp404160y | J. Phys. Chem. B 2013, 117, 8408−8421

Table 7. Highest Spearman and Pearson Correlation Coefficients (r_s and r_p) and the Corresponding Solute Dielectric Constants for the MM/PBSA calculations with Different Partial Charges for Ligands Based on the 0.2−1 ns MD Trajectories

	RESP		AM1-BCC		ESP		GAS	
	r_s	r_p	r_s	r_p	r_s	r_p	r_s	r_p
avidin	ε_{in} = 1	ε_{in} = 1	ε_{in} = 1	ε_{in} = 1	ε_{in} = 1	ε_{in} = 1	ε_{in} = 1	ε_{in} = 1
	1.00	0.95	0.89	0.91	0.96	0.95	0.21	0.69
human thrombin	ε_{in} = 2	ε_{in} = 2	ε_{in} = 4	ε_{in} = 4	ε_{in} = 4	ε_{in} = 4	ε_{in} = 4	ε_{in} = 4
	0.79	0.77	0.61	0.64	0.54	0.41	0.5	0.33
neuraminidase	ε_{in} = 4	ε_{in} = 4	ε_{in} = 4	ε_{in} = 4	ε_{in} = 4	ε_{in} = 4	ε_{in} = 4	ε_{in} = 4
	0.69	0.72	0.81	0.70	0.38	0.38	0.17	0.00
Pim-1 kinase	ε_{in} = 2	ε_{in} = 2	ε_{in} = 1	ε_{in} = 1	ε_{in} = 1	ε_{in} = 1	ε_{in} = 4	ε_{in} = 2
	0.66	0.66	0.74	0.76	0.73	0.74	0.59	0.57
SYK	ε_{in} = 2	ε_{in} = 4	ε_{in} = 4	ε_{in} = 4	ε_{in} = 4	ε_{in} = 2	ε_{in} = 2	ε_{in} = 1
	0.55	0.52	0.44	0.19	0.72	0.69	0.69	0.91
ranking score	3.69		3.49		3.33		2.16	

MM/PBSA based on shorter MD simulations (Table 6). The RESP charges give the best ranking score (3.25) among the four types of partial charges employed by MM/GBSA. Our observations are not surprising because the RESP charges are optimized from the ESP charges, and they are less conformation-dependent than the RESP charges and can avoid the problem of large ESP charges that may be problematic for simulating intramolecular interactions.[40] The AM1-BCC charges were designed to reproduce atomic charges that emulate the electrostatic potential at the HF/6-31G* level of theory for small molecules based on a set of optimized parameters. According to our predictions, the ranking capability of the AM1-BCC charges (ranking score = 3.18) is even better than that of the ESP charges (ranking score = 3.09), and only slightly worse than that of the RESP charges. The little difference in the ranking scores between the RESP and AM1-BCC charges suggests that the AM1-BCC charges show quite good compatibility with the ff03 force field and are good replacements of the RESP charges in MD simulations and free energy calculations.

According to the comparison study (Table 6), the Gasteiger charges yield the worst ranking results (ranking score = 1.85). The Gasteiger charges only give reasonable results for Pim1 kinase and SYK (Figure 5). As mentioned above, the Gasteiger charges are derived from an empirical approach, and they are apparently not compatible with the ff03 force field in most cases. Therefore, although the Gasteiger charge model has been widely used in virtual screening, it is not a good choice for the MM/PBSA and MM/GBSA calculations implemented in AMBER.

A comparison was also made for MM/PBSA based on the four methods of obtaining partial charges. As shown in Table 7, the RESP charges still show the best performance, the AM1-BCC and ESP charges also give comparable ranking results, and the Gasteiger charges yield the worst predictions. In numerous cases the AM1-BCC partial charges have shown comparative prediction capability with the RESP charges.[33,43,49] Our results also illustrate that the predictions based on the AM1-BCC charges are satisfactory and they are only slightly worse than those based on the RESP charges. Moreover, for two systems (Pim1 kinase and SYK), the AM1-BCC charges even give better predictions than the RESP charges (Figure 5A and B).

For all of the four types of charges, compared with MM/GBSA (GB^{OBC1}), MM/PBSA with the *pbsa* module always gives better predictions to rank the binding affinities (Figure 5). In summary, MM/PBSA based on the RESP charges makes the best predictions for ranking the inhibitors, and MM/PBSA based on the AM1-BCC charges also gives comparative results. Considering the high computational efficiency, the AM1-BCC charge model is the best choice for screening large-scale compound libraries.

CONCLUSION

We examined the impact of five force fields and four methods of deriving partial charges for small molecules on the binding free energies predicted by the MM/GBSA and MM/PBSA approaches. Our conclusions are as follows:

(1) For MM/GBSA with GB^{OBC1}, the ff99 force field gives the best results when using middle time-scale MD simulations (4 ns), and the ff03 force field gives the best results when using short time-scale MD simulations (1 ns). Overall, the ff03 force field is the best choice for most cases when no precedents can be learned and short time-scale simulations are performed, such as the processing of docking results as studied by our previous work.[46]

(2) When middle time-scale MD simulations are performed, such as 2−4 ns, the ff99 or ff12SB force field may be a good choice as mentioned above, while the other tested force fields will be recommended for short MD simulations (1 ns or less); however, the simulation time is heavily system-dependent. For rigid systems with only one binding position of the ligands, such as the systems investigated in this study, a longer MD simulation, for example, 10 ns, may not be necessary to achieve better predictions, if only the binding energies need to be calculated.

(3) For most cases, MM/PBSA with the *pbsa* program and Lu's radii set gives better ranking results than MM/GBSA with GB^{OBC1}. For shorter MD simulations (1 ns), the ff03 force field yields the best results by MM/PBSA as it does by MM/GBSA; while for middle time-scale MD simulations (4 ns), the ff99SB force field is the best choice for MM/PBSA.

(4) Based on shorter MD simulations (1 ns), we found that the RESP charge, with no doubt, is the best for the MM/GBSA and MM/PBSA calculations with the AMBER force fields, while the AM1-BCC and ESP charge also afford comparative predictions. Due to the high computational efficiency, the AM1-BCC charges are preferred for screening large-scale compound libraries by short MD simulations and MM/GBSA.

Our study gives a systematic evaluation of the impact of force fields for proteins, time scale of MD simulations, methods of obtaining partial charges for small molecules, and binding free

dx.doi.org/10.1021/jp404160y | J. Phys. Chem. B 2013, 117, 8408−8421

energy calculation methods on ranking binding free energies for five sets of inhibitors. Our results are useful for selecting proper force field and ligand charges for binding free energy calculation based on relatively short MD simulations (≤10 ns).

■ ASSOCIATED CONTENT

Supporting Information

Figure S1. 2-D structures of the studied inhibitors: (a1−a7) avidin inhibitors, (b1−b7) human thrombin inhibitors, (c1−c8) neuraminidase inhibitors, (d1−d16) Pim1 kinase inhibitors, (e1−e8) SYK inhibitors; **Table S1.** The PDB entries and experimental binding free energies for the studied systems. This material is available free of charge via the Internet at http://pubs.acs.org.

■ AUTHOR INFORMATION

Corresponding Author

*E-mail: tingjunhou@hotmail.com or tjhou@suda.edu.cn. Phone: +86-512-65882039.

Author Contributions

Lei Xu and Huiyong Sun are co-first authors.

Notes

The authors declare no competing financial interest.

■ ACKNOWLEDGMENTS

This study was supported by the National Science Foundation of China (21173156), the National Basic Research Program of China (973 program, 2012CB932600), and the Priority Academic Program Development of Jiangsu Higher Education Institutions (PAPD).

■ REFERENCES

(1) Hou, T. J.; Guo, S. L.; Xu, X. J. Predictions of Binding of A Diverse Set of Ligands to Gelatinase-A by A Combination of Molecular Dynamics and Continuum Solvent Models. *J. Phys. Chem. B* **2002**, *106*, 5527−5535.

(2) Gohlke, H.; Kiel, C.; Case, D. A. Insights into Protein-Protein Binding by Binding Free Energy Calculation and Free Energy Decomposition for The Ras-Raf and Ras-Ralgds Complexes. *J. Mol. Biol.* **2003**, *330*, 891−914.

(3) Gohlke, H.; Klebe, G. Approaches to The Description and Prediction of The Binding Affinity of Small-Molecule Ligands to Macromolecular Receptors. *Angew. Chem., Int. Ed.* **2002**, *41*, 2644−2676.

(4) Hou, T.; Xu, Z.; Zhang, W.; McLaughlin, W. A.; Case, D. A.; Xu, Y.; Wang, W. Characterization of Domain-Peptide Interaction Interface A Generic Structure-Based Model to Decipher The Binding Specificity of SH3 Domains. *Mol. Cell. Proteomics* **2009**, *8*, 639−649.

(5) Hou, T.; Yu, R. Molecular Dynamics and Free Energy Studies on The Wild-Type and Double Mutant HIV-1 Protease Complexed with Amprenavir and Two Amprenavir-Related Inhibitors: Mechanism for Binding and Drug Resistance. *J. Med. Chem.* **2007**, *50*, 1177−1188.

(6) Hou, T.; Zhang, W. Characterization of Domain-Peptide Interaction Interface: A Case Study on The Amphiphysin-1 SH3 Domain. *J. Mol. Biol.* **2008**, *376*, 1201−1214.

(7) Hou, T.; Zhang, W.; Wang, J.; Wang, W. Predicting Drug Resistance of The HIV-1 Protease Using Molecular Interaction Energy Components. *Proteins: Struct., Funct., Bioinf.* **2009**, *74*, 837−846.

(8) Hou, T. J.; Li, N.; Li, Y. Y.; Wang, W. Characterization of Domain-Peptide Interaction Interface: Prediction of SH3 Domain-Mediated Protein-Protein Interaction Network in Yeast by Generic Structure-based Models. *J. Proteome Res.* **2012**, *11*, 2982−2995.

(9) Hou, T. J.; Li, Y. Y.; Wang, W. Prediction of Peptides Binding to The PKA RII Alpha Subunit Using A Hierarchical Strategy. *Bioinformatics* **2011**, *27*, 1814−1821.

(10) Hou, T. J.; Zhu, L. L.; Chen, L. R.; Xu, X. J. Mapping The Binding Site of A Large Set of Quinazoline Type EGF-R Inhibitors Using Molecular Field Analyses and Molecular Docking Studies. *J. Chem. Inf. Comput. Sci.* **2003**, *43*, 273−287.

(11) Huo, S.; Massova, I.; Kollman, P. A. Computational Alanine Scanning of The 1: 1 Human Growth Hormone-Receptor Complex. *J. Comput. Chem.* **2002**, *23*, 15−27.

(12) Huo, S.; Wang, J.; Cieplak, P.; Kollman, P. A.; Kuntz, I. D. Molecular Dynamics and Free Energy Analyses of Cathepsin D-Inhibitor Interactions: Insight into Structure-Based Ligand Design. *J. Comput. Chem.* **2002**, *45*, 1412−1419.

(13) Kuhn, B.; Kollman, P. A. Binding of A Diverse Set of Ligands to Avidin And Streptavidin: An Accurate Quantitative Prediction of Their Relative Affinities by A Combination of Molecular Mechanics and Continuum Solvent Models. *J. Med. Chem.* **2000**, *43*, 3786−3791.

(14) Liu, H.; Yao, X. Molecular Basis of The Interaction for An Essential Subunit PA-PB1 in Influenza Virus RNA Polymerase: Insights from Molecular Dynamics Simulation and Free Energy Calculation. *Mol. Pharmaceut.* **2009**, *7*, 75−85.

(15) Liu, H.; Yao, X.; Wang, C.; Han, J. In Silico Identification of The Potential Drug Resistance Sites over 2009 Influenza A (H1N1) Virus Neuraminidase. *Mol. Pharmaceut.* **2010**, *7*, 894−904.

(16) Muzzioli, E.; Del Rio, A.; Rastelli, G. Assessing Protein Kinase Selectivity with Molecular Dynamics and MM-PBSA Binding Free Energy Calculations. *Chem. Biol. Drug Des.* **2011**, *78*, 252−259.

(17) Wang, J.; Morin, P.; Wang, W.; Kollman, P. A. Use of MM-PBSA in Reproducing The Binding Free Energies to HIV-1 RT Of TIBO Derivatives and Predicting The Binding Mode to HIV-1 RT of Efavirenz by Docking and MM-PBSA. *J. Am. Chem. Soc.* **2001**, *123*, 5221−5230.

(18) Xu, L.; Li, Y.; Zhou, S.; Hou, T. Understanding Microscopic Binding of Macrophage Migration Inhibitory Factor with Phenolic Hydrazones by Molecular Docking, Molecular Dynamics Simulations and Free Energy Calculations. *Mol. BioSyst.* **2012**, *8*, 2260−2273.

(19) Xu, Z.; Hou, T.; Li, N.; Xu, Y.; Wang, W. Proteome-wide Detection of Abl1 SH3-binding Peptides by Integrating Computational Prediction and Peptide Microarray. *Mol. Cell. Proteomics* **2012**, *11*, O111.010389.

(20) Xue, W.; Pan, D.; Yang, Y.; Liu, H.; Yao, X. Molecular Modeling Study on The Resistance Mechanism of HCV NS3/4A Serine Protease Mutants R155K, A156V and D168A to TMC435. *Antiviral Res.* **2011**, *93*, 126−137.

(21) Page, C. S.; Bates, P. A. Can MM-PBSA Calculations Predict The Specificities of Protein Kinase Inhibitors? *J. Comput. Chem.* **2006**, *27*, 1990−2007.

(22) Wang, W.; Lim, W. A.; Jakalian, A.; Wang, J.; Wang, J.; Luo, R.; Bayly, C. I.; Kollman, P. A. An Analysis of The Interactions Between The Sem-5 SH3 Domain and Its Ligands Using Molecular Dynamics, Free Energy Calculations, and Sequence Analysis. *J. Am. Chem. Soc.* **2001**, *123*, 3986−3994.

(23) Homeyer, N.; Gohlke, H. Free Energy Calculations by The Molecular Mechanics Poisson-Boltzmann Surface Area Method. *Mol. Informatics* **2012**, *31*, 114−122.

(24) Kollman, P. A.; Massova, I.; Reyes, C.; Kuhn, B.; Huo, S. H.; Chong, L.; Lee, M.; Lee, T.; Duan, Y.; Wang, W.; Donini, O.; Cieplak, P.; Srinivasan, J.; Case, D. A.; Cheatham, T. E. Calculating Structures and Free Energies of Complex Molecules: Combining Molecular Mechanics and Continuum Models. *Acc. Chem. Res.* **2000**, *33*, 889−897.

(25) Wang, J. M.; Hou, T. J.; Xu, X. J. Recent Advances in Free Energy Calculations with A Combination of Molecular Mechanics and Continuum Models. *Curr. Comput.-Aided Drug Des.* **2006**, *2*, 287−306.

(26) Beveridge, D. L.; DiCapua, F. Free Energy via Molecular Simulation: Applications to Chemical and Biomolecular Systems. *Annu. Rev. Biophys. Biomol. Struct.* **1989**, *18*, 431−492.

(27) Jorgensen, W. L.; Thomas, L. L. Perspective on Free-Energy Perturbation Calculations for Chemical Equilibria. *J. Chem. Theory Comput.* **2008**, *4*, 869−876.

(28) Sitkoff, D.; Sharp, K. A.; Honig, B. Accurate Calculation of Hydration Free Energies Using Macroscopic Solvent Models. *J. Phys. Chem. B* **1994**, *98*, 1978−1988.

(29) Onufriev, A.; Bashford, D.; Case, D. A. Exploring Protein Native States and Large-Scale Conformational Changes with A Modified Generalized Born Model. *Proteins: Struct., Funct., Bioinf.* **2004**, *55*, 383−394.
(30) Zhang, W.; Hou, T.; Xu, X. New Born Radii Deriving Method for Generalized Born Model. *J. Chem. Inf. Model.* **2005**, *45*, 88−93.
(31) Zhang, W.; Hou, T.; Qiao, X.; Xu, X. Parameters for The Generalized Born Model Consistent with RESP Atomic Partial Charge Assignment Protocol. *J. Phys. Chem. B* **2003**, *107*, 9071−9078.
(32) Hou, T.; Wang, J.; Li, Y.; Wang, W. Assessing The Performance of The MM/PBSA and MM/GBSA Methods: I. The Accuracy of Binding Free Energy Calculations Based on Molecular Dynamics Simulations. *J. Chem. Inf. Model.* **2011**, *51*, 69−82.
(33) Genheden, S.; Ryde, U. Comparison of End-Point Continuum-Solvation Methods for The Calculation of Protein−Ligand Binding Free Energies. *Proteins: Struct., Funct., Bioinf.* **2012**, *80*, 1326−1342.
(34) Cornell, W. D.; Cieplak, P.; Bayly, C. I.; Gould, I. R.; Merz, K. M.; Ferguson, D. M.; Spellmeyer, D. C.; Fox, T.; Caldwell, J. W.; Kollman, P. A. A Second Generation Force Field for The Simulation of Proteins, Nucleic Acids, and Organic Molecules. *J. Am. Chem. Soc.* **1995**, *117*, 5179−5197.
(35) Wang, J.; Cieplak, P.; Kollman, P. A. How Well Does A Restrained Electrostatic Potential (RESP) Model Perform in Calculating Conformational Energies of Organic and Biological Molecules? *J. Comput. Chem.* **2000**, *21*, 1049−1074.
(36) Hornak, V.; Abel, R.; Okur, A.; Strockbine, B.; Roitberg, A.; Simmerling, C. Comparison of Multiple Amber Force Fields and Development of Improved Protein Backbone Parameters. *Proteins: Struct., Funct., Bioinf.* **2006**, *65*, 712−725.
(37) Lindorff-Larsen, K.; Piana, S.; Palmo, K.; Maragakis, P.; Klepeis, J. L.; Dror, R. O.; Shaw, D. E. Improved Side-Chain Torsion Potentials for The Amber ff99sb Protein Force Field. *Proteins: Struct., Funct., Bioinf.* **2010**, *78*, 1950−1958.
(38) Duan, Y.; Wu, C.; Chowdhury, S.; Lee, M. C.; Xiong, G.; Zhang, W.; Yang, R.; Cieplak, P.; Luo, R.; Lee, T. A Point-Charge Force Field for Molecular Mechanics Simulations of Proteins Based on Condensed-Phase Quantum Mechanical Calculations. *J. Comput. Chem.* **2003**, *24*, 1999−2012.
(39) Case, D. A.; Darden, T. A.; Cheatham, T. E., III; Simmerling, C. L.; Wang, J.; Duke, R. E.; Luo, R.; Walker, R. C.; Zhang, W.; Merz, K. M. *AMBER*, 12th ed.; University of California, San Francisco, 2012.
(40) Bayly, C. I.; Cieplak, P.; Cornell, W.; Kollman, P. A. A Well-Behaved Electrostatic Potential Based Method Using Charge Restraints for Deriving Atomic Charges: The RESP Model. *J. Phys. Chem.* **1993**, *97*, 10269−10280.
(41) Weiner, S. J.; Kollman, P. A.; Case, D. A.; Singh, U. C.; Ghio, C.; Alagona, G.; Profeta, S.; Weiner, P. A New Force Field for Molecular Mechanical Simulation of Nucleic Acids and Proteins. *J. Chem. Theory Comput.* **1984**, *106*, 765−784.
(42) Jakalian, A.; Jack, D. B.; Bayly, C. I. Fast, Efficient Generation of High-Quality Atomic Charges. AM1-BCC Model: II. Parameterization and Validation. *J. Comput. Chem.* **2002**, *23*, 1623−1641.
(43) Mobley, D. L.; Dumont, É.; Chodera, J. D.; Dill, K. A. Comparison of Charge Models for Fixed-Charge Force Fields: Small-Molecule Hydration Free Energies in Explicit Solvent. *J. Phys. Chem. B* **2007**, *111*, 2242−2254.
(44) Genheden, S. MM/GBSA and LIE Estimates Of Host−Guest Affinities: Dependence on Charges and Solvation Model. *J. Comput.-Aided Mol. Des.* **2011**, *25*, 1085−1093.
(45) Gasteiger, J.; Marsili, M. Iterative Partial Equalization of Orbital Electronegativity—A Rapid Access to Atomic Charges. *Tetrahedron* **1980**, *36*, 3219−3228.
(46) Hou, T.; Wang, J.; Li, Y.; Wang, W. Assessing The Performance of The Molecular Mechanics/Poisson Boltzmann Surface Area and Molecular Mechanics/Generalized Born Surface Area Methods. II. The Accuracy of Ranking Poses Generated from Docking. *J. Comput. Chem.* **2011**, *32*, 866−877.
(47) Weis, A.; Katebzadeh, K.; Söderhjelm, P.; Nilsson, I.; Ryde, U. Ligand Affinities Predicted with The MM/PBSA Method: Dependence on The Simulation Method and The Force Field. *J. Med. Chem.* **2006**, *49*, 6596−6606.
(48) Genheden, S.; Kuhn, O.; Mikulskis, P.; Hoffmann, D.; Ryde, U. The Normal-Mode Entropy in The MM/GBSA Method: Effect of System Truncation, Buffer Region, and Dielectric Constant. *J. Chem. Inf. Model.* **2012**, *52*, 2079−2088.
(49) Rizzo, R. C.; Aynechi, T.; David, A.; Kuntz, I. D. Estimation of Absolute Free Energies of Hydration Using Continuum Methods: Accuracy of Partial Charge Models and Optimization of Nonpolar Contributions. *J. Chem. Theory Comput.* **2006**, *2*, 128−139.
(50) Gross, K. C.; Seybold, P. G.; Hadad, C. M. Comparison of Different Atomic Charge Schemes for Predicting Pka Variations in Substituted Anilines and Phenols. *Int. J. Quantum Chem.* **2002**, *90*, 445−458.
(51) JonesHertzog, D. K.; Jorgensen, W. L. Binding Affinities for Sulfonamide Inhibitors with Human Thrombin Using Monte Carlo Simulations with A Linear Response Method. *J. Med. Chem.* **1997**, *40*, 1539−1549.
(52) Farmer, L. J.; Bemis, G.; Britt, S. D.; Cochran, J.; Connors, M.; Harrington, E. M.; Hoock, T.; Markland, W.; Nanthakumar, S.; Taslimi, P. Discovery and SAR of Novel 4-Thiazolyl-2-Phenylaminopyrimidines As Potent Inhibitors of Spleen Tyrosine Kinase (SYK). *Bioorg. Med. Chem. Lett.* **2008**, *18*, 6231−6235.
(53) Pugliese, L.; Coda, A.; Malcovati, M.; Bolognesi, M. Three-Dimensional Structure of The Tetragonal Crystal form Of Egg-White Avidin in Its Functional Complex with Biotin at 2.7 A Resolution. *J. Mol. Biol.* **1993**, *231*, 698−710.
(54) Banner, D. W.; Hadvary, P. Crystallographic Analysis at 3.0-A Resolution of The Binding to Human Thrombin of Four Active Site-Directed Inhibitors. *J. Biol. Chem.* **1991**, *266*, 20085−20093.
(55) Pierce, A. C.; Jacobs, M.; Stuver-Moody, C. Docking Study Yields Four Novel Inhibitors of the Protooncogene Pim-1 Kinase. *J. Med. Chem.* **2008**, *51*, 1972−1975.
(56) SYBYL molecular simulation package; http://www.sybyl.com.
(57) Frisch, M. J.; Trucks, G. W.; Schlegel, H. B.; Scuseria, G. E.; Robb, M. A.; Cheeseman, J. R.; Montgomery, J. A. J.; Vreven, T.; Kudin, K. N.; Burant, J. C.; Millam, J. M.; Lyengar, S. S.; Tomasi, J.; Barone, V.; Mennucci, B.; Cossi, M.; Scalmani, G.; Rega, N.; Petersson, G. A.; Nakatsuji, H.; Hada, M.; Ehara, M.; Toyota, K.; Fukuda, R.; Hasegawa, J.; Ishida, M.; Nakajima, T.; Honda, Y.; Kitao, O.; Nakai, H.; Klene, M.; Li, X.; Knox, J. E.; Hratchian, H. P.; Cross, J. B.; Bakken, B.; Adamo, C.; Jaramillo, J.; Gomperts, R.; Stratmann, R. E.; Yazyev, O.; Austin, A. J.; Cammi, R.; Pomelli, C.; Ochterski, J. W.; Ayala, P. Y.; Morokuma, K.; Voth, G. A.; Salvador, P.; Dannenberg, J. J.; Zakrzewski, V. G.; Dapprich, S.; Daniels, A. D.; Strain, M. C.; Farkas, O.; Malick, D. K.; Rabuck, A. D.; Raghavachari, K.; Foresman, J. B.; Ortiz, J. V.; Cui, Q.; Baboul, A. G.; Clifford, S.; Cioslowski, J.; Stefanov, B. B.; Liashenko, A.; Liashenko, A.; Piskorz, P.; Komaromi, I.; Martin, R. L.; FOx, D. J.; Keith, T.; Al-Laham, M. A.; Peng, C. Y.; Nanayakkara, A.; Challacombe, M.; Gill, P. M. W.; Johnson, B.; Chen, W.; Wong, M. W.; Gonzalez, C.; Pople, J. A. *Gaussian 09*; Gaussian Inc.; Wallingford, CT, 2009.
(58) Wang, J.; Wang, W.; Kollman, P. A.; Case, D. A. Automatic Atom Type and Bond Type Perception in Molecular Mechanical Calculations. *J. Mol. Graphics Model.* **2006**, *25*, 247−260.
(59) Walker, R. C.; Crowley, M. F.; Case, D. A. The Implementation of A Fast and Accurate QM/MM Potential Method in Amber. *J. Comput. Chem.* **2008**, *29*, 1019−1031.
(60) Wang, J.; Wolf, R. M.; Caldwell, J. W.; Kollman, P. A.; Case, D. A. Development and Testing of A General Amber Force Field. *J. Comput. Chem.* **2004**, *25*, 1157−1174.
(61) Jorgensen, W. L.; Chandrasekhar, J.; Madura, J. D.; Impey, R. W.; Klein, M. L. Comparison of Simple Potential Functions for Simulating Liquid Water. *J. Chem. Phys.* **1983**, *79*, 926−935.
(62) Case, D. A., Darden, T. A., Cheatham, T. E., III, Simmerling, C. L., Wang, J., Duke, R. E., Luo, R., Walker, R. C., Zhang, W., Merz, K. M., Roberts, B., Hayik, S., Roitberg, A., Seabra, G., Swails, J., Goetz, A. W., Kolossváry, I., Wong, K. F., Paesani, F., Vanicek, J., Wolf, R. M., Liu, J., Wu, X., Brozell, S. R., Steinbrecher, T., Gohlke, H., Cai, Q., Ye, X., Wang, J., Hsieh, M.-J., Cui, G., Roe, D. R., Mathews, D. H., Seetin, M. G.,

Salomon-Ferrer, R., Sagui, C., Babin, V., Luchko, T., Gusarov, S., Kovalenko, A., Kollman, P. A. *AMBER 12*; University of California, San Francisco, 2012.
(63) Darden, T.; York, D.; Pedersen, L. Particle Mesh Ewald: An N.Log (N) Method for Ewald Sums in Large Systems. *J. Chem. Phys.* **1993**, *98*, 10089−10092.
(64) Andersen, H. C. Molecular Dynamics Simulations at Constant Pressure and/or Temperature. *J. Chem. Phys.* **1980**, *72*, 2384−2393.
(65) Ryckaert, J. P.; Ciccotti, G.; Berendsen, H. J. C. Numerical Integration of The Cartesian Equations of Motion of A System with Constraints: Molecular Dynamics of N-Alkanes. *J. Comput. Phys.* **1977**, *23*, 327−341.
(66) Weiser, J.; Shenkin, P. S.; Still, W. C. Approximate Atomic Surfaces from Linear Combinations of Pairwise Overlaps (LCPO). *J. Comput. Chem.* **1999**, *20*, 217−230.
(67) Luo, R.; David, L.; Gilson, M. K. Accelerated Poisson−Boltzmann Calculations for Static And Dynamic Systems. *J. Comput. Chem.* **2002**, *23*, 1244−1253.
(68) Lu, Q.; Luo, R. A Poisson−Boltzmann Dynamics Method with Nonperiodic Boundary Condition. *J. Chem. Phys.* **2003**, *119*, 11035−11048.
(69) Tan, C.; Yang, L.; Luo, R. How Well Does Poisson-Boltzmann Implicit Solvent Agree with Explicit Solvent? A Quantitative Analysis. *J. Phys. Chem. B* **2006**, *110*, 18680−18687.
(70) Rocchia, W.; Alexov, E.; Honig, B. Extending The Applicability of The Nonlinear Poisson-Boltzmann Equation: Multiple Dielectric Constants and Multivalent Ions. *J. Phys. Chem. B* **2001**, *105*, 6507−6514.